Indian Journal of Pure & Applied Physics
Vol. 64, April 2026, pp. 349-357
DOI: 10.56042/ijpap.v64i4.20488

Improved Performance of Organic Light Emitting Diodes by Balanced Charge Injection

Aparna Tripathi[a*], Pankaj Kumar[b] & V S Pandey[a]

[a]National Institute of Technology Delhi, GT Karnal Road, Delhi 110036, India

[b]CSIR-National Physical Laboratory, Dr. K. S. Krishnan Road, New Delhi 110012, India

Received: 9th June 2025; accepted: 9th February 2026

Balanced charge injection in organic light emitting diodes (OLEDs) has been investigated towards improving their efficiency and stability. Balanced charge injection was achieved through selective insertion and elimination of some charge injection and charge transport layers. Poly(ethylene-dioxythiophene):poly(styrenesulfonate) (PEDOT:PSS) was used as hole injecting layer (HIL) but because of its hygroscopic nature, it caused rapid degradation in device performance. Elimination of PEDOT:PSS and insertion of thin films of hole transporting N,N′-Di (1-naphthyl)-N,N′-diphenyl- (1,1′-biphenyl)-4,4′-diamine (NPD), and hole blocking bathocuproine (BCP) along with electron injecting 8-hydroxyquinolinolato-lithium (Liq) layer led to balanced charge injection into light emitting tri(8-hydroxyquinolinato) aluminium (Alq3) layer that resulted in improved current efficiency (CE) of OLEDs. The reference device with PEDOT:PSS showed maximum CE of 0.4 cd/A, whereas the device with balanced charge injection exhibited much enhanced CE of 1.75 cd/A. Furthermore, after ~15 h of continuous operation, the reference device retained only ~15% of its initial CE whereas the device with balanced charge injection retained over 80% of its initial CE, demonstrating substantially improved operational stability by balanced charge injection.

Keywords: Thin films, OLEDs, Alq3, Charge transport layers, Balanced injection, Degradation, Stability

1 Introduction

Organic light-emitting diodes (OLEDs) were first prepared in 1987 by Tang and VanSlyke[1]. Although the initial performance of OLEDs was not appreciable but their potential as an alternative light-emitting technology and their wide range of applications motivated extensive research and development efforts worldwide. OLEDs offer several advantages over conventional light-emitting technologies, including their ultra-thin structure, light weight, mechanical flexibility, wider viewing angle, high resolution, fast response time, low power consumption and cost-effectiveness. Their mechanical flexibility enables them to be fabricated on a variety of flexible substrates such as flexible glass, thin plastic sheets, thin metal foils, papers, and even fabrics[2-4]. In addition, OLEDs can be fabricated over large areas using conventional printing techniques, including 3D printing methods[5, 6]. These features make OLEDs a leading candidate for next-generation flat-panel displays and solid-state lighting applications[7-10]. Thanks to their excellent features and global research and developmental work, OLEDs are now available in the market[11-17]. Currently, intensive research efforts are focused on improving the efficiency and operational stability of OLEDs, particularly white OLEDs, as they are considered ideal for high-resolution full-color displays and general lighting applications[15,18].

An OLED typically consists of two electrodes, called anode and cathode, with one or more organic semiconducting layers sandwiched between them. At least one of the electrodes is optically transparent that allows the emitted light to come out of the device. Under forward bias, cathode injects electrons whereas anode injects holes into the light emitting organic layer. The injected electrons and holes form excitons, which may decay either radiatively or non-radiatively. Radiative decay of excitons results in light emission, whereas non-radiative decay leads to heat generation. In case of imbalanced charge injection, the excess charge carriers do not form excitons, therefore contribute only to the electrical current and not to the light emission. For efficient device operation, high injection of charge carriers at low operating voltages is required, but excess of any of the charge carriers adversely affects device performance. The charge carriers that do not participate in exciton formation,

*Corresponding author: E-mail: aparnatripathi@nitdelhi.ac.in

form polarons and participate in exciton quenching and enhance non-radiative recombination. The polarons generate heat through resistive losses within the device. Heating accelerates material degradation and reduces device operational lifetime. Therefore, achieving balanced charge injection is essential for high-performance OLEDs. Phosphorescent and thermally activated delayed fluorescent (TADF) OLEDs are very efficient as both the singlet and triplet excitons there can decay radiatively but in case of fluorescent OLEDs only single excitons decay radiative. Fluorescent OLEDs exhibit very low efficiency and stability compared to phosphorescent and TADF materials based OLEDs[19-25]. For efficient and stable OLEDs, apart from spin statistics and type of exciton formation, the ratio of the injected charge carriers is also important. The charge injection is strongly influenced by the work functions of the electrode materials, energies of highest occupied molecular orbitals (HOMOs) and lowest unoccupied molecular orbitals (LUMOs) of organic semiconductors and their electronic properties. Energy level mismatches at material interfaces act as energy barriers to charge injection. These energy barriers behave as internal series resistances, which lead to imbalanced charge injection and Joule heating in the devices. Therefore, for high-performance OLEDs, interface energy barriers should be minimized while maintaining the balanced charge injection into the emissive layer.

The efficiency and operational stability of OLEDs has been improved here by balancing the charge injection and recombination within the emissive layer. Charge balance was realized through strategic insertion and elimination of selected charge transport and charge injection layers. Since green-emitting OLEDs have widespread applications including traffic signals, sign boards, digital displays, building decorations and full colour displays, we used green light emitting Alq3 as the emissive material for present studies. The reference OLED device, comprising PEDOT:PSS as HIL and Alq3 as emissive layer, exhibited maximum CE of 0.4 cd/A and showed rapid degradation under continuous operation at a constant applied voltage. Insertion of a hole transport layer (HTL) between PEDOT:PSS and Alq3 layers balanced the injected charge densities that not only improved the CE but also increased the device stability by partially protecting the Alq3 layer from hygroscopic PEDOT:PSS[26]. Elimination of PEDOT: PSS and insertion a very thin hole blocking and electron injecting layers after Alq3 layer, further improved the charge balance and improved the device operational stability. The best device structure with better charge balance, exhibited maximum CE of 1.75 cd/A and much better stability than the reference device. While the CE of the reference device dropped to 57% of its initial value within 30 minutes of continuous operation, the optimized device with balanced charge injection retained more than 80 % of its initial efficiency even after 17 hours of continuous operation at a constant applied voltage. These results demonstrate that OLEDs can achieve higher efficiency and superior stability through balanced charge injection, even if the charge injection is balanced through higher interface barriers.

2 Experimental Methods

2.1 Materials

Indium tin oxide (ITO) coated glass sheets (sheet resistance 15 Ω/□), poly(ethylene-dioxythiophene): poly(styrene sulfonate) (PEDOT:PSS) (1.3 wt% aqueous solution), N,N′-Di (1-naphthyl)-N,N′-diphenyl-(1,1′-biphenyl)-4,4′-diamine (NPD) (96%), tri(8-hydroxyquinolinato) aluminium (Alq3) (98%), bathocuproine (BCP) (96%) and aluminium metal(Al) (99.99%) were purchased from Sigma Aldrich, USA, whereas 8-Hydroxyquinolinato-lithium (Liq) (98%) was purchased from Tokyo Chemical Industry (TCI), Japan. Figure 1 shows chemical structures of the materials used in the present study. ITO coated glass sheets were cut into 25 × 25 mm^2 size substrates and each substrate was patterned using a laser scriber to have two 6 mm wide and 25 mm long stripes. All other materials were used as received.

2.2 Fabrication of OLEDs

OLEDs were fabricated on pre-patterned ITO coated glass substrates. ITO served as an optically transparent anode that allowed the emitted light to come out of the device. Prior to device fabrication, the substrates were cleaned using a standard cleaning procedure[27]. Initially, the substrates were ultrasonicated in a soap solution for 15 min and then subsequently rinsed thoroughly with deionized (DI) water. This was followed by sequential ultrasonication in acetone and isopropanol for 15 min each. The substrates were then dried using a high-pressure nitrogen (N_2) gun and treated with air plasma for 15 min to enhance the ITO work function and improve its surface wettability. For fabrication of OLEDs we used a number of organic materials, which

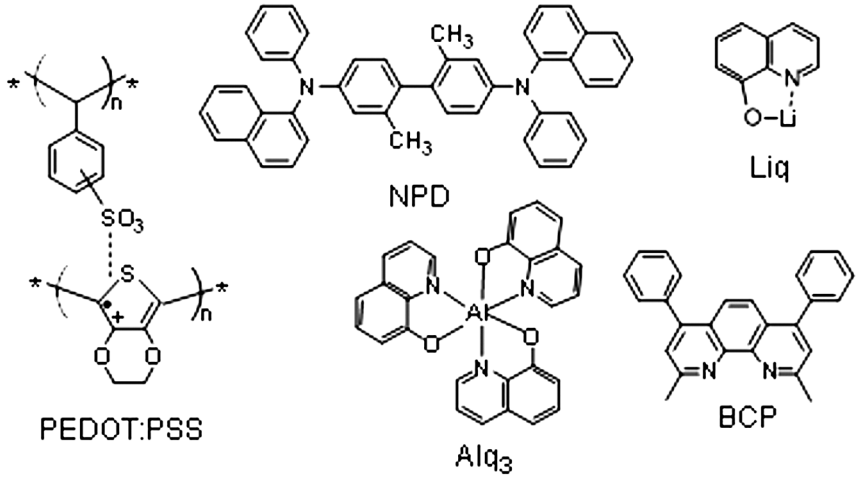

Fig. 1 — Chemical structure of the materials used in the present study

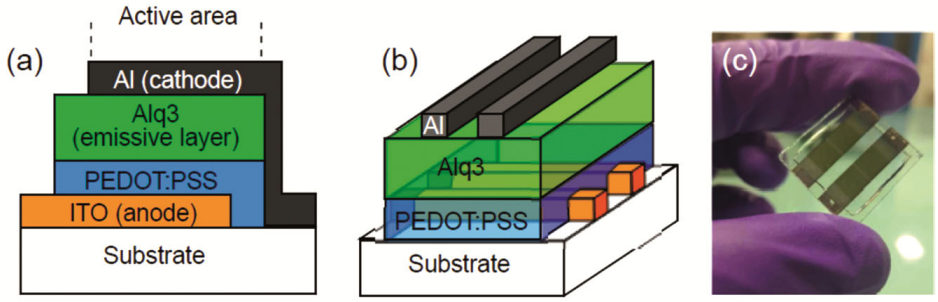

Fig. 2 — Schematic (a) 2D and (b) 3D representation of the structure of the reference OLED device (c) photograph of one of the OLEDs device

played different roles in device operation and stability. Alq3 was used as green light emitting material for present studies. Initially, we prepared OLEDs in the structure ITO/PEDOT:PSS/Alq3 (35 nm)/Al (100 nm) (reference device). Later on, to improve device efficiency and stability, the device architecture was systematically engineered by incorporating different charge transport and buffer layers. The following devices were prepared:

Reference device: ITO/PEDOT: PSS/Alq3 (35 nm)/Al (100 nm).
Device A: ITO/PEDOT:PSS/NPD (35 nm)/Alq3 (35 nm)/Al (100 nm).
Device B: ITO/NPD (35 nm)/Alq3 (35 nm)/Al (100 nm).
Device C: ITO/NPD (35 nm)/Alq3 (35 nm)/BCP (5 nm)/Liq (2 nm)/Al (100 nm).

Here ITO works as hole injecting anode and Al works as electron injecting cathode. Thin films of PEDOT:PSS were deposited by spin coating at 4000 rpm for 1 min, followed by annealing at 150°C for 30 min on a hot plate. Thin films of all other organic materials, as well as Al metal electrodes, were deposited by thermal evaporation through shadow masks in a high-vacuum chamber at a base pressure of 2×10^{-6} mbar. All organic materials were deposited at 0.2-0.5 Å/s in the organic evaporation chamber without breaking vacuum and the Al electrodes were deposited at 1 Å/s in a separate metal evaporation chamber. Film thicknesses and their deposition rates were monitored using a quartz crystal thickness monitor. Al electrodes with a thickness of 100 nm were deposited in cross geometry with the ITO electrodes. Each substrate contained four pixels and each pixel had the active area of 0.36 cm^2. Figures 2 (a) and (b) respectively illustrate the two-dimensional (2D) and three-dimensional (3D) schematic structures of the reference OLED device, while Fig. 2(c) shows a photograph of a fabricated OLED. After fabrication, all devices were encapsulated inside a nitrogen-filled glove box with moisture (H_2O) content < 1 ppm and oxygen (O_2) concentration of 320 ppm. Encapsulation was performed using glass cover slips and UV-curable epoxy. The epoxy was applied to the cover slips, which were then placed over the OLED samples in such a way that they covered all active areas

of the samples except the substrate edges where from we took the contacts for device testing. The samples were subsequently exposed to UV light for 10 min to cure the epoxy, thereby protecting the devices from ambient O_2 and H_2O.

2.3 Characterization of OLEDs

The OLEDs were characterized for their electroluminescence (EL), Commission Internationale de l'Éclairage (CIE) coordinates, current density–voltage (*J-V*), and luminance-voltage (*L-V*) characteristics. The EL spectra and CIE coordinates were recorded using an Ocean Optics HR4000 spectrometer. The *J-V* characteristics were measured using a Keithley 2450 SourceMeter, while the *L-V* characteristics were obtained using a Keithley 2450 SourceMeter in combination with a Konica Minolta LS160 luminance meter. All the characterization tools were interfaced with computer and operated by their respective softwares. Under forward bias, electrons inject from cathode and holes inject from anode. The injected charge carriers transport through the respective transport layers and recombine in the emissive layer to emit light. The *J-V* and *L-V* characteristics were used to calculate the CE of each device. To study the degradation in current density and luminance, a constant voltage was continuously applied to the device, and the current densities and luminance values were recorded at regular time intervals. Measurements of current density and luminance at each point enabled us to calculate the degradation in CE. The applied constant voltage for each device was adjusted to achieve an initial luminance of 100 cd/m^2. Since the devices exhibited different performance characteristics, the applied constant voltage, to get initial luminance of 100 cd/m^2 for each device was different.

3 Results and Discussion

Figure 3 shows the EL spectrum of the reference OLED device that spanned from 450 nm to 675 nm with an emission peak at 523 nm. Inset of Fig. 3 shows the CIE chromaticity diagram, which represents the color purity of the emitted light. The CIE coordinates of the reference device were found to be (0.31, 0.54), which corresponded to a correlated color temperature (CCT) of 5990 K. The position of the CIE coordinates on the chromaticity diagram has been shown by open circle and indicated by an arrow. Figure 4 shows the *J-V* and *L-V* characteristics of the reference device, measured up to 8 V. The turn-on voltage (V_{ON}), the voltage at which the luminance reached 1 cd/m^2, was observed to be 3.0 V. Both luminance and current density increased nonlinearly with the applied voltage. At lower voltages, the increment in luminance was gradual; but beyond 4 V, the luminance increased rapidly. However, at higher voltages the increment slowed, and beyond 7.5 V the luminance began to decrease. The current density increased slowly up to 4 V and then sharply at higher voltages. The increment in luminance can be attributed to the increased injected charge carrier density, but for better understanding of reduction in luminance at higher voltages, the CE was calculated. The variation of CE with applied voltage is shown in the inset of Fig. 4. The CE first increased with applied

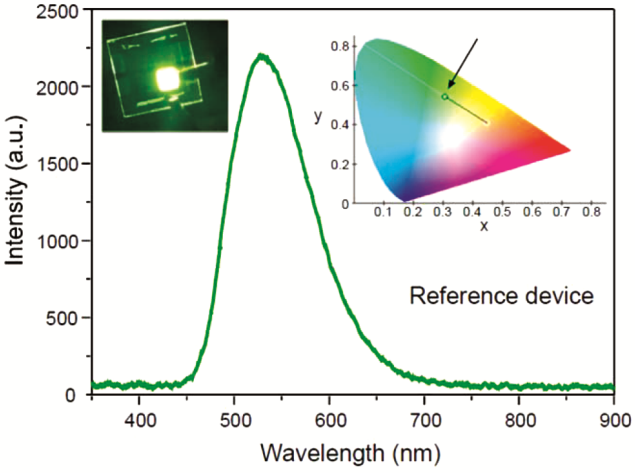

Fig. 3 — EL spectrum of the reference OLED device. Inset on the right hand side shows the position of CIE coordinates of the emitted light on the chromaticity diagram whereas the inset on the left hand side shows the photograph of the OLED under operation

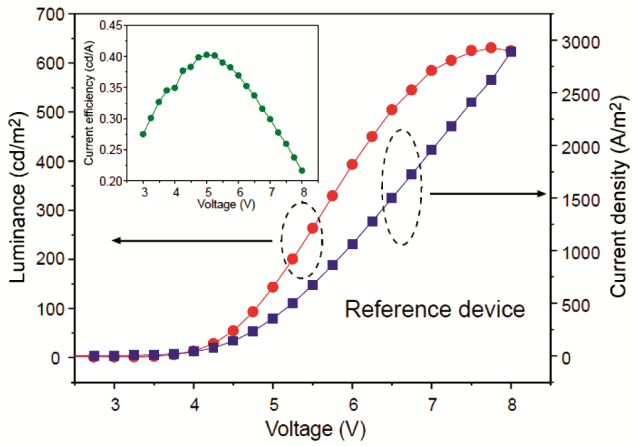

Fig. 4 — *J-V* and *L-V* characteristics of the reference OLED device. Inset shows the variation of CE as a function of applied voltage

voltage, reached a maximum value of 0.4 cd/A at 5 V, and then decreased at higher voltages. Since Alq3 exhibit higher electron mobility than its hole mobility, the recombination zone in the reference device is formed near the PEDOT:PSS/Alq3 interface that results in quenching of excitons and low CE. The luminance at 5 V was 143.1 cd/m^2. The increment in CE at low voltages can be attributed to improved electron-hole recombination due to increased charge injection, but the subsequent reduction in CE at higher operating voltages is likely due to charge-injection imbalance, non-radiative recombination and heat-induced degradation.

It is worth noting that increment in the applied voltage enhances the injection of charge carriers; however, due to the presence of different energy barriers at various interfaces, the increments in injected electrons and holes are not similar. Because of imbalanced injection of charge carriers, the number of emitted photons does not increase proportionately, and the rate of increment in the luminance decreases at higher currents. Figure 5 schematically shows the HOMO and LUMO energy levels of different materials used in this study. From the energy-level diagram, for the reference device an energy barrier of approximately 0.7 eV is expected at the PEDOT:PSS/Alq3 interface, while a larger barrier of about 1.3 eV exists at the Alq_3/Al interface. The energy barriers at the organic-organic and metal-organic interfaces act as series resistances and the bulk resistivity of the organic layers also contributes to the overall series resistance in the device. The series resistance in the device leads to Joule heating. At an applied voltage of 7 V, the current density of reference device exceeded 1900 A/m², which is quite a high current density for such devices and the Joule heating leads to degradation in Alq3 and other organic layers. To verify if the high injection current density resulted in degradation in Alq3 molecules, the *L-V* characteristics of the same device were measured for multiple times. Figure 6 shows the *J-V* and *L-V* characteristics of the reference device measured for multiple scans taken one after other. With each successive scan, both the current density and luminance decreased. The reduction in current density clearly indicates deterioration in the electronic properties of the device, which can be attributed to the formation of inactive ("dead") zones in the active area due to heat-induced degradation caused by the large current density flowing through the device. Since such thermally induced degradation processes are irreversible, the device performance degraded progressively with each subsequent scan.

The stability of the devices was also investigated under continuous operation at constant applied voltages. For stability studies of reference device, a constant voltage of 4.9 V was applied to another reference device that resulted in initial luminance of 100 cd/m^2, and the current density and luminance were measured at regular time intervals. Figure 7 shows the normalized degradation profiles of the current density, luminance, and CE of the reference device. Both the current density and luminance exhibited a rapid decrease during the initial hour of operation. Within the first 30 minutes, the current density dropped to 49 % of its initial value, while the luminance decreased more sharply to 28 % of its initial value, resulting in a reduction of CE to 57 % of its initial value. After that the degradation rates of both current density and luminance slowed down. The decay in luminance can be attributed to reduced electron-hole recombination resulting from the

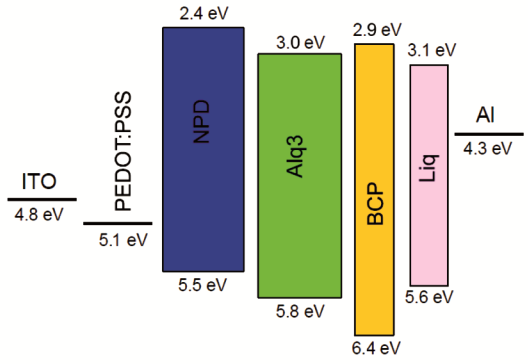

Fig. 5 — Schematic energy level diagram of the OLED device incorporating different materials used in the present study

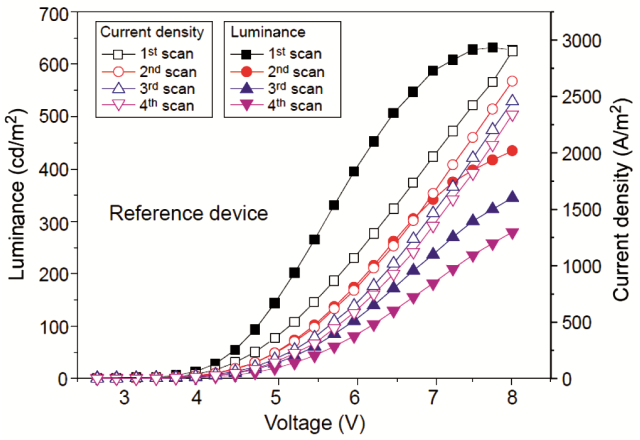

Fig. 6 — *J-V* and *L-V* characteristics of the reference OLED device for multiple scans taken one after other

reduced injection of charge carriers. However, the observed reduction in luminance was significantly larger than the reduction in current density, indicating an imbalanced decay of injected charge carriers. Such imbalance in charge carriers promotes non-radiative recombination, thereby reducing the radiative efficiency of the device. It is important to note that PEDOT:PSS is a hygroscopic material that readily absorbs moisture from the environment that can subsequently diffuse into the adjacent Alq3 layer. O_2 and moisture are highly detrimental to organic semiconductors. Exposure to O_2 and H_2O molecules, leads to chemical decomposition and degradation in both the electrical and optical properties of organic semiconductors[28]. In the present study, PEDOT:PSS films were spin-coated in air and then transferred to a vacuum chamber for thermal deposition of other layers. During this process, it is likely that the PEDOT:PSS film absorbed some environmental moisture. The absorbed moisture degrades the electrical properties of PEDOT:PSS, and since Alq3 was in direct contact with PEDOT:PSS, the moisture adsorb by PEDOT:PSS also diffused into Alq3 layer and degraded its properties as well. Degradation in organic molecules gets accelerated under applied electric field. In addition, the moisture will also oxidized Al electrode at the Alq3/Al interface, creating an additional barrier for electron injection. As a result, the number of electrons injected into the Alq3 layer will reduced and cause further charge imbalance. Degradation in PEDOT:PSS reduces hole injection into Alq3. The combined reduction in injected electrons and holes leads to reduction in both the current density and luminance. Furthermore, exciton quenching at the PEDOT:PSS/Alq3 interface becomes significant under these degraded conditions, which further suppresses the device efficiency[28].

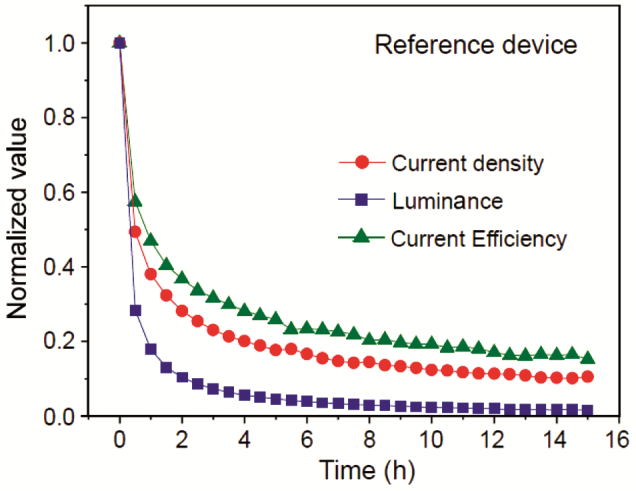

Fig. 7 — Degradation profiles of the normalized current density, luminance and CE of the reference OLED device under continuous operation at 4.9 V

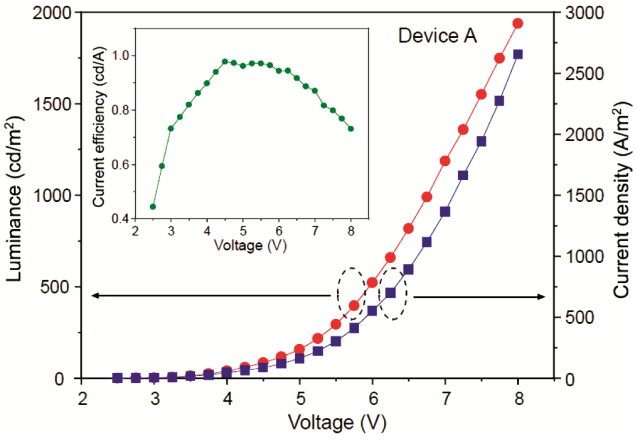

Fig. 8 — *J-V* and *L-V* characteristics of Device A. Inset shows the plot of its CE as a function of applied voltages

To mitigate the adverse impact of PEDOT:PSS on device stability, a thin layer of NPD was inserted in between PEDOT:PSS and Alq3 layers and Device A was prepared. NPD served here as HTL. Insertion of a thin HTL with higher hole mobility shifts the recombination zone within the emissive layer away from the PEDOT:PSS interface, thereby reducing exciton quenching. The EL spectrum and CIE coordinates of Device A were similar to those of the reference device and are therefore not shown here. Figure 8 shows the *J-V* and *L-V* characteristics of Device A, while the inset shows the variation in its CE with applied voltage. At a given applied voltage, Device A exhibited lower current density but higher luminance compared to the reference device. The combination of reduced current and enhanced luminance resulted in a significantly higher CE for Device A. The CE initially increased with applied voltage, reached a maximum value of 0.97 cd/A at 4.5 V, and then decreased at higher voltages. The observed reduction in current and enhancement in luminance for Device A, relative to the reference device, can be explained from the energy levels of different materials, shown in Fig. 5. NPD layer introduces an additional series resistance for hole injection into Alq3 and it also blocks some electrons going from Alq3 to PEDOT:PSS without radiative recombination. By reducing the number of injected holes and confining electrons within the Alq3 layer,

NPD layer helps in balancing the electron-hole ratio in Alq3, and improves the CE. Unlike the reference device, Device A did not exhibit a reduction in luminance at higher operating voltages, even though the current density through it was still quite high. Although the Joule heating due to internal series resistance and heat-induced degradation were still present, the improved charge balance prevented reduction in luminance. In addition, the incorporation of the NPD layer significantly enhanced the operational stability of Device A.

Figure 9 shows the normalized degradation profiles of current density, luminance, and CE of Device A under continuous operation at a constant applied voltage of 4.75 V. Device A was applied 4.75 V to get initial luminance of 100 cd/m^2. Both the current density and luminance reduced with time; however, the rates of reduction were substantially lower than those observed for the reference device. The luminance decreased to 50 % of its initial value after 12.5 h, while the current density at that time retained 61 % of its initial value. The improved stability of Device A can be attributed to the protection of Alq3 by NPD from PEDOT:PSS film, thereby mitigating moisture-induced degradation. As observed PEDOT:PSS was injecting too much of holes into the device, which appeared to be good at the first instance but from charge balance point of view it was not good. Moreover, due to its hygroscopic nature we thought of removing PEDOT:PSS completely from the device and Device B was prepared. The EL spectrum and CIE coordinates of Device B were also similar to those of the reference device and are therefore not shown here. Figure 10 shows the *J-V* and *L-V* characteristics of Device B. A drastic reduction in the device current density was observed, which can be attributed to a significant decrease in hole injection. In the absence of PEDOT:PSS, the hole injection barrier at the ITO/NPD interface increased from 0.4 eV to 0.7 eV (Fig. 5), which decreased the hole injection. The variation of CE with applied voltage for Device B is shown in the inset of Fig. 10. Notably, Device B exhibited a maximum CE of 1.17 cd/A at an applied voltage of 7.75 V. Enhancement in CE can be attributed to a more balanced injection of electrons and holes into the Alq3 layer. Having achieved improved efficiency through the reduction of hole injection, Further enhancement of device efficiency was sought by increasing electron injection into the Alq_3 layer. To reduce the electron-injection barrier at the Alq3/cathode interface, thin layers of BCP (5 nm) and Liq (2 nm) were introduced in between Alq3 and the Al cathode and Device C was fabricated. The EL spectrum and CIE coordinates of Device C as well were similar to those of the reference device and are therefore not shown here. The *J-V* and *L-V* characteristics of Device C are also shown in Fig. 10, and the variation in its CE with applied voltage is represented in the inset. At all applied voltages, Device C exhibited higher CE than Device B, indicating improved charge balance due to enhanced electron injection. The maximum CE of Device C reached 1.75 cd/A at an applied voltage of 8 V. A comparison of the key performance parameters of the reference device and Devices A, B, and C is

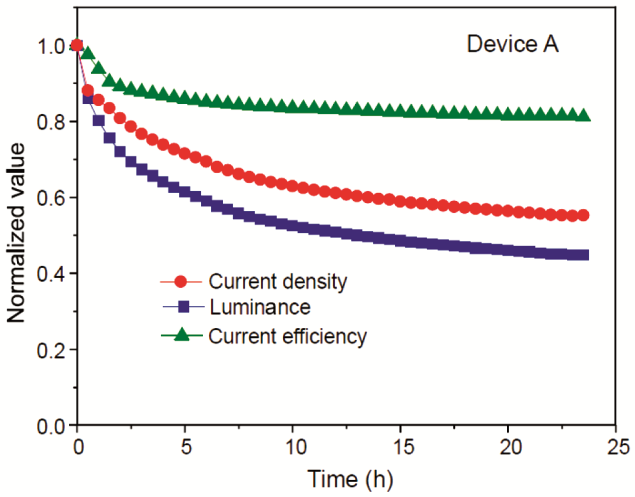

Fig. 9 — Degradation profiles of the normalized current density, luminance and CE of Device A under continuous operation at 4.75 V

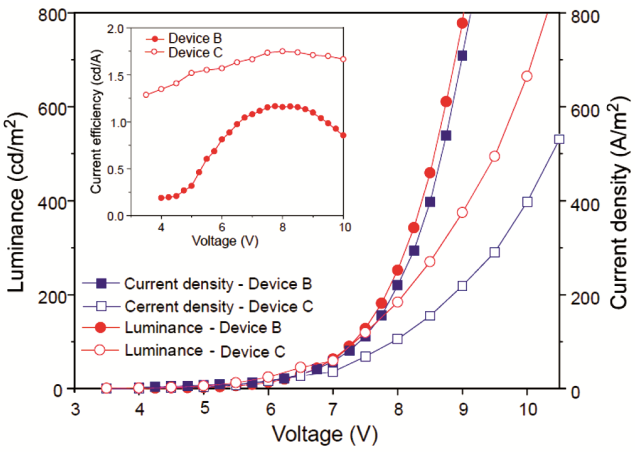

Fig. 10 — *J-V* and *L-V* characteristics of Device B and Device C. Inset shows the plots of their CE as a function of applied voltages

Table 1 — Characteristics performance parameters of the reference device and Devices A, B and C

Device	V_{ON}* (V)	Maximum CE	CIE coordinates	CCT (K)
Reference device	3.0	0.4 cd/A @ 5.0 V	(0.31, 0.54)	5990
Device A	2.5	0.97 cd/A @ 4.5 V	(0.32, 0.54)	5960
Device B	2.5	1.17 cd/A @ 7.5 V	(0.32, 0.53)	5951
Device C	2.5	1.75 cd/A @ 8 V	(0.32, 0.54)	5970

*Voltage at which the device luminance was 1 cd/m^2

Table 2 — CEs of Alq3 based OLEDs with different HIL, HTL, ETL and EIL films. The bottom electrode was ITO and the top electrode was Al in all these devices

HIL	HTL	ETL	EIL	CE (cd/A)	Reference
-	TPD	-	LiF	0.80	[26]
-	NPD	-	Ca	2.47	[29]
-	NPD	BPhen	LiF	3.37	[30]
PEDOT:PSS	-	-	-	2.21	[31]
-	TPD	-	-	2.90	[31]
MoO_3	NPD:MoO_3	-	LiF	0.27	[32]
MoO_3	NPD:MoO_3/NPD	-	LiF	2.79	[32]
NiO	-	-	LiF	0.2	[33]
-	NPD	BCP	Liq	1.75	This work

TPD = N,N′-Bis (3-methylphenyl)-N,N′-diphenylbenzidine, BPhen = Bathophenanthroline, LiF = Lithoum fluoride, MoO_3 = Molybdenum oxide, NiO = Nickel oxide

summarized in Table 1. The performance of these devices was comparable to the Alq3 based OLEDs reported in the literature[26, 29-33]. The comparison of CE of our optimized device (Device C) with CEs of Alq3 based OLEDs reported in the literature, is given in Table 2.

The improved efficiency of Device C can be attributed to more balanced electron-hole injection and recombination within the Alq3 layer. Compared to Device B, Device C exhibited reduced current density, which arose from the hole-blocking behavior of the BCP layer due to high HOMO-HOMO energy barrier at the Alq3/BCP interface. This high interfacial barrier confines holes within the Alq3 layer. The accumulation of holes leads to the formation of a space-charge field, which inhibits further hole injection and consequently reduces the device current. In principle a thin layer of Liq dopes BCP layer with Li+ ions, which reduces the electron injection barrier at the cathode interface. The reduced injection barrier at cathode enhances electron injection from cathode into the Alq3 layer, resulting in increased electron-hole recombination at comparatively lower currents. As a result of this improved charge balance, Device C exhibited the highest CE among all the devices studied. Beyond efficiency enhancement, Device C also demonstrated superior operational stability. Figure 11 shows the normalized degradation profiles of current density, luminance, and CE of Device C under continuous operation at a constant applied voltage of 7.25 V. Device C exhibited initial luminance of 100 cd/m^2 at 7.25 V. Although both current density and luminance decreased with time, the degradation rates were slower than those observed for the other devices. After 17 h of continuous operation, the luminance decreased to only 52.5 % of its initial value, while the current density decreased to only 65.5 % of its initial value. Notably, after 15 h of operation, where the CE of the reference device dropped to approximately 15 % of its initial value, Device C retained nearly 80% of its initial CE.

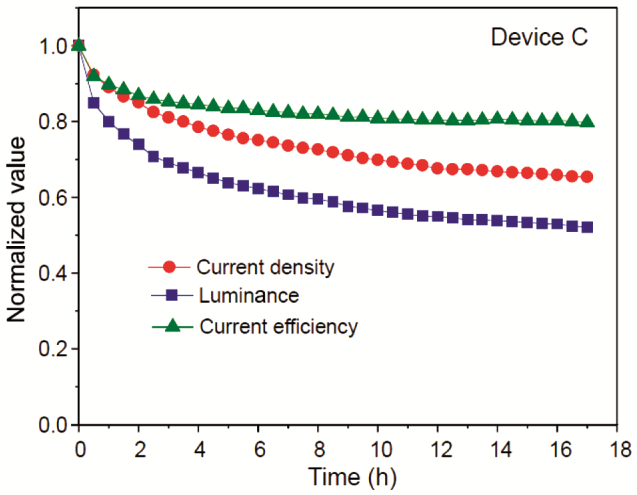

Fig. 11 — Degradation profiles of the normalized current density, luminance and CE of Device C under continuous operation at 7.25 V

4 Conclusion

Both the efficiency and stability of OLEDs were significantly improved by achieving balanced charge injection and recombination within the emissive layer. The reference device exhibited a CE of 0.4 cd/A, however, just within 30 min of continuous operation, its current density and luminance dropped rapidly to 49 % and 28 % of their initial values, respectively. Insertion of NPD between PEDOT:PSS and Alq3 layers resulted in simultaneous enhancement in CE and operational lifetime of the device. This improvement is attributed to effective isolation of the emissive layer from the hygroscopic PEDOT:PSS and balanced charge injection in Alq3. Further removal of PEDOT:PSS, along with insertion of a hole-blocking BCP layer and an electron-injecting Liq layer (Device C), led to additional enhancement in both the CE and device stability. Device C exhibited CE of 1.75 cd/A and even after 17 h of continuous operation, it retained over 65 % of its initial current density and over 52 % of its initial luminance. Notably, compared to the reference device, Device C retained nearly 20 times higher CE after 15 h of continuous operation. These results clearly demonstrate that careful control of charge injection and recombination is an effective strategy for simultaneously improving the efficiency and operational stability of OLEDs.

Acknowledgement

The work reported in this paper was carried out under a Department of Science and Technology (DST), Govt. of India sponsored WOS-A project (DST/WOS-A/PM-90/2021).

References

1 Tang C W & VanSlyke S A, *Appl Phys Lett*, 51 (1987) 913.
2 Jang H J, Lee J Y, Kwak J, Lee D, Park J H, Lee B & Noh YY, *J Inform Disp*, 20 (2019) 1.
3 Choi S, Kang C, Byun C W, Cho H, Kwon B H, Han J H, Yang J H, Shin J W, Hwang C S, Cho N S, Lee K M, Kim H O, Kim E, Yoo S & Lee H, *Nat Commun*, 11 (2020) 2732.
4 Nam M, Chang J, Kim H, Son Y H, Jeon Y, Kwon J H & Choi K C, *npj Flex Electron*, 8 (2024) 17.
5 Su R, Park S H, Ouyang X, Ahn S I & Mcalpine M C, *Sci Adv*, 8 (2022) eabl8798.
6 Kant C, Shukla A, McGregor S K M, Lo S C, Namdas E B & Katiyar M, *Nature Commun*,14 (2023) 7220.
7 Su Q, Zhang H & Chen S, *npj Flex Electron*, 5 (2021) 8.
8 Jia S, Tang H, Ma J, Ding S, Qu X, Xu B, Wu Z, Li G, Liu P, Wang K & Sun XW, *Adv Opt Mater*, 9 (2021) 2101069.
9 Jun H Y, Kim S J & Choi CH, *Nanomater*, 11 (2021) 3441.
10 Chen HW, Lee J H, Lin B Y, Chen S & Wu S T, *Light Sci Appl*, 7 (2018) 17168.
11 Dickson G, *Information Display*, 39 (2023) 21.
12 Misra A, Kumar P, Kamalasanan M N & Chandra S, *Semicond Sci Technol*, 21 (2006) R35.
13 Misra A, Kumar P, Srivastava R, Dhawan S K, Kamalasanan MN & Chandra S, *Ind J Pure & App Phys*, 43 (2005) 921.
14 Kalyani N T & Dhoble S J, *Renew & Sustain Energy Rev*, 16 (2012) 2696.
15 Tripathi A & Kumar P, *Ind J Pure & Appl Phys*, 60 (2022) 105.
16 Wu Z & Ma D, *Mater Sci Enging R: Reports*, 107 (2016) 1.
17 Zou S J, Shen Y, Xie FM, Chen J D, Li YQ & Tang J X, *Mater Chem Front*, 4 (2020) 788.
18 Wu S F, Li S H, Wang Y K, Huang C C, Sun Q, Liang J J, Liao L S & Fung MK, *Adv Funct Mater*, 27 (2017) 1701314.
19 Dai X & Cao J, *Org Electron*, 78 (2020) 105563.
20 Zhang G, Xing G, Lang J, Li C, Wang X & Wang D, *Opt Commun*, 459 (2020) 124921.
21 Zhang Q, Tsang D, Kuwabara H, Hatae Y, Li B, Takahashi T, Lee SY, Yasuda T & Adachi C, *Adv Mater*, 27 (2015) 2096.
22 Tripathi A & Kumar P, *Ind J Pure & Appl Phys*, 60 (2022) 415.
23 Uoyama H, Goushi K, Shizu K, Nomura H & Adachi C, *Nature*, 492 (2012) 234.
24 Dias FB, Bourdakos K N, Jankus V, Moss KC, Kamtekar KT, Bhalla V, Santos J, Bryce MR & Monkman AP, *Adv Mater*, 25 (2013) 3707.
25 Miao Y & Yin M, *iSci*, 25 (2022) 103804.
26 Lee Y, Biswas S & Kim H, *Thin Solid Films*, 746 (2022) 139134.
27 Kumar P, Misra A, Bhardwaj R, Kamalasanan M N, Jain S C, Chand S & Tandon R P, *Displays*, 29 (2008) 351.
28 Naqvi S M K A, Baig M F, Farid T, Nazir Z, Mohsan S A H, Liu Z, Cai W & Chang S, *Nanomater*, 13 (2023) 3020.
29 Kim H J, Tamura T, Nakayama Y, Noguchi Y & Ishii H, *J Photopolym Sci Technol*, 25 (2012) 183.
30 Cai M, Xiao T, Liu R, Chen Y, Shinar R & Shinar J, *Appl Phys Lett*, 99 (2011) 153303.
31 Wang G F, Tao X M & Wang R X, *Comp Sci Technol*, 68 (2008) 2837.
32 Zhao Y, Su J, Zou W, Wu Y, Zhang C & Shao M, *Next Mater*, 6 (2025) 100426.
33 Chan I M & Hong F C, *Thin Solid Films*, 450 (2004) 304.